Contents lists available at ScienceDirect

Inorganica Chimica Acta

journal homepage: www.elsevier.com/locate/ica

Research paper

The human YAE1-ORAOV1 complex of the cytosolic iron-sulfur protein assembly machinery binds a [4Fe-4S] cluster

Nihar Ranjan Prusty [a], Francesca Camponeschi [a], Simone Ciofi-Baffoni [a,b,*], Lucia Banci [a,b,*]

[a] Magnetic Resonance Center CERM, University of Florence, Via Luigi Sacconi 6, 50019, Sesto Fiorentino, Florence, Italy
[b] Department of Chemistry, University of Florence, Via della Lastruccia 3, 50019 Sesto Fiorentino, Florence, Italy

ARTICLE INFO

ABSTRACT

Iron-sulfur (Fe-S) clusters are among the most versatile cofactors in biology. Although Fe-S clusters formation can be achieved spontaneously *in vitro* with inorganic iron and sulfur sources, the *in vivo* behaviour is more complex and requires the so-called Fe-S biogenesis machineries. In the cytosol, the biogenesis of Fe-S proteins is assisted by the cytosolic Fe-S protein assembly machinery, which comprises at least thirteen known proteins, among which there are human ORAOV1 and YAE1. A hetero-complex formed by the two latter proteins facilitates Fe-S cluster insertion in the human ABC protein ABCE1 within a chain of binding events that are still not well understood. In the present work, ORAOV1 and the YAE1-ORAOV1 complex were produced and their structural and cluster binding properties spectroscopically investigated. It resulted that both ORAOV1 and the YAE1-ORAOV1 complex are characterized by well-structured, α-helical regions and by unstructured, flexible regions, and are both able to bind a $[4Fe-4S]^{2+}$ cluster. Bioinformatics and site-directed mutagenesis studies indicated that the $[4Fe-4S]$ cluster in ORAOV1 is bound by a conserved cluster binding motif, while YAE1, which does not have a metal-binding consensus motif, is not essential for the $[4Fe-4S]^{2+}$ cluster binding in the YAE1-ORAOV1 hetero-complex. Overall, these results support a model that the YAE1-ORAOV1 complex might actively participate in the Fe-S cluster insertion into ABCE1 thanks to the $[4Fe-4S]^{2+}$ cluster binding properties of ORAOV1.

1. Introduction

Iron-sulfur (Fe-S) clusters are crucial cofactors for life [1,2]. They are involved in a tremendous number of reactions at the basis of cellular metabolic processes. The structural complexity of the Fe-S clusters and their potential toxicity for the cellular environment has resulted in complex machineries, operative in both prokaryotic and eukaryotic organisms, for assembling Fe-S clusters, delivering and inserting them into the final target proteins, which require Fe-S cluster(s) for their function [3–6]. In eukaryotic cells, these sophisticated machineries operate in different cellular compartments. Thus, differentiated machineries are present in each cellular compartment. In non-plant eukaryotes, the action of two composite proteinaceous machineries coordinate the maturation of Fe-S proteins in mitochondria and in the cytosol, respectively.

The CIA machinery that comprises at least thirteen known proteins assists the maturation of Fe-S proteins in the cytosol [7]. Two

contrasting models have emerged to describe cytoplasmic Fe-S protein maturation. The main difference between the two models relies on the dependence or independence of Fe-S cluster formation in the CIA machinery from the mitochondrial iron-sulfur cluster machinery. One model proposes the existence of a *de novo* cytosolic ISC pathway in mammalian cells, which can supply the elemental components (i.e., iron and sulfur) and the biogenesis proteins required to build the cluster in the cytosol of mammalian cells [5,8,9]. On the contrary, the second model proposes that the assembly of extra-mitochondrial Fe-S proteins relies on the mitochondrial ISC machinery for the synthesis of a still chemically undefined, sulfur-containing compound that is exported to the cytoplasm by the ABC transporter ABCB7 in human and utilized for the assembly of a [4Fe-4S] cluster on a complex formed by two two-homologous P-loop ATPases termed NUBP1 and NUBP2 [10,11]. In this second model, the cluster synthesis on the latter complex requires two [2Fe-2S] clusters, which are donated by GLRX3 (i.e. the [2Fe-2S] cluster

chaperone of the CIA machinery [12,13]) and two electrons, which have been proposed to be provided by the electron transfer chain composed by the flavin-dependent oxidoreductase NDOR1 and the Fe-S protein CIAPIN1 [14–17]. The next step in the second model of the CIA machinery involves the trafficking of the NUBP1-NUBP2 assembled [4Fe-4S] cluster that, owing to its exposed coordination, is bound in a rather labile fashion [12,18]. This step requires another CIA machinery component, the CIAO3 protein, which was proposed to receive the assembled [4Fe-4S] cluster for delivering it to the CIA targeting complex, composed by three proteins, i.e. CIAO2B, CIAO1 and MMS19 [19–22], whose 3D structure has been recently solved [23]. The latter complex is devoted to insert the [4Fe-4S] cluster received by CIAO3 into final target proteins that operate both in the cytosol and in the nucleus. The current understanding is, indeed, that nuclear apo target proteins receive their clusters in the cytosol, and are subsequently imported into the nucleus as holo-proteins.

Some cytosolic Fe-S target proteins follow a maturation pathway that includes additional accessory proteins responsible of their biogenesis. One of these cases concerns the maturation mechanism operative for the human ABC protein ABCE1, a protein coordinating two [4Fe-4S] clusters, which is involved in the biosynthesis of the ribosome as well as in several aspects of ribosome function [24–28]. This protein requires all mentioned CIA components for the maturation of its two [4Fe-4S] clusters bound at a *N*-terminal ferredoxin-like domain [29]. Furthermore, the maturation depends also on a 'CIA adapter complex' composed of ORAOV1 (oral cancer-overexpressed protein 1) and YAE1 (Yae1 domain-containing protein 1) [28,30]. These proteins interact each other mainly via sequential GX_3 motifs, present on both proteins, which are evolutionarily conserved at their *N*-termini but not found in any other eukaryotic protein. The present molecular model is that the 'CIA adapter complex' escorts the apo form of ABCE1 to the CIA targeting complex, thus allowing facile cluster transfer from the CIA targeting complex to ABCE1. However, which is the specific role of the CIA adapter complex, i.e. whether the complex actively participates in the Fe-S cluster binding and insertion into ABCE1 or not, is yet undetermined. In this work, we have investigated *in vitro* the cluster binding properties of ORAOV1 and of the 'CIA adapter complex' through an approach that combines bioinformatics, site-directed mutagenesis, NMR, EPR and UV–visible spectroscopies.

2. Experimental

2.1. Sequence search and analysis

ORAOV1 and YAE1 homologous sequences were searched for in the GenBank Databases (CDS translations + PDB + SwissProt + PIR + PRF) using sequence similarity criteria with a threshold of 20%. This was accomplished by starting from human ORAOV1 and YAE1 sequences and performing a protein BLAST search using standard parameters. Sequence alignments were performed with CLUSTALW [31] and WebLogo [32].

2.2. Cloning, expression and purification of apo and holo ORAOV1

The cDNA coding for human ORAOV1 (UniProtKB/Swiss-Prot: Q8WV07) was acquired from Genewiz, and was inserted into the pTH34 vector, using the Gateway® technology (Invitrogen) to express ORAOV1 with a N-terminal β-1 Immunoglobulin Binding Domain of Protein G (GB1)-His$_6$ tag (pTH34-ORAOV1, hereafter). BL21 (DE3) gold competent *E. coli* cells were transformed with the pTH34-ORAOV1 plasmid and cells were grown in LB or in M9 minimal medium containing 1 mM ampicillin at 37 °C under vigorous shaking up to a cell OD$_{600}$ of 0.6. Protein expression was induced by adding 0.5 mM IPTG and cells were grown overnight at 17 °C. Cells were harvested by centrifugation at 7500 × g and resuspended in 40 mM sodium phosphate buffer pH 8.0, 300 mM NaCl, 20 mM imidazole, 3 mM DTT, 0.01 mg/mL DNase, 0.01

mg/mL lysozyme, 20 mM MgSO$_4$, protease inhibitor cocktail (Sigma Aldrich) and 10% (v/v) glycerol. Cell disruption was performed on ice by sonication. The soluble extract, obtained by ultracentrifugation at 40000×*g*, was loaded on a HisTrap FF column (GE Healthcare) and the recombinant protein was eluted with 40 mM sodium phosphate buffer pH 8.0, 300 mM NaCl, 400 mM imidazole, 0.2 mM EDTA, 3 mM DTT and concentrated with an Amicon Ultra-15 Centrifugal Filter Units with a MWCO of 10 kDa (Millipore), after addition of 5 mM DTT. The protein was buffer exchanged in 40 mM sodium phosphate buffer pH 8.0, 300 mM NaCl, 5 mM imidazole by PD-10 desalting column. Cleavage of the GB1-His$_6$ tag was performed by TEV protease overnight at room temperature. The protein solution was loaded on a HisTrap FF column to separate the digested protein from the tag and TEV protease. After concentration, the protein was buffer exchanged in 50 mM sodium phosphate buffer pH 8.0, 200 mM NaCl and 5 mM DTT and stored at 4 °C in μM concentration range.

Chemical reconstitution of ORAOV1 was performed in an anaerobic chamber (O$_2$ < 1 ppm), by incubating the apo protein for 6 h at room temperature in degassed 50 mM Tris, 200 mM NaCl, 5 mM DTT, at pH 8.0 with up to an 8-fold excess of FeCl$_3$ and Na$_2$S. Excess of FeCl$_3$ and Na$_2$S was anaerobically removed by passing the mixture on a PD-10 desalting column, and the holo protein was recovered.

2.3. AMS-based alkylation gel shift assay

A gel shift assay on samples previously modified with AMS was performed as previously reported [33]. AMS reacts with available thiol groups, resulting in a mobility shift of the protein on SDS-PAGE due to its increase in size of 0.5 kDa per added AMS molecule. Specifically, ORAOV1 protein was precipitated with 10% (v/v) trichloroacetic acid in the presence and in the absence of 5 mM DTT, followed by washing with acetone. The samples were resuspended in 40 mM phosphate buffer pH 8.0, 200 mM NaCl and 8 M urea, and were incubated with 10 mM AMS for 30 min at 25 °C, followed by 10 min at 37 °C. Samples were checked by non-reducing SDS-PAGE, and the gel was stained with Coomassie Blue.

2.4. Cloning, expression and purification of apo and holo forms of the YAE1-ORAOV1 complex

The pRSFDuet-1 co-expression vector containing the cDNA coding for human ORAOV1 (UniProtKB/Swiss-Prot: Q8WV07) and human YAE1 (UniProtKB/Swiss-Prot: Q9NRH1) (pRSFDuet-1-YAE1-ORAOV1 plasmid, hereafter) was acquired from source Twin Helix. YAE1 and ORAOV1 genes were inserted, respectively, between *Eco*RI and *Not*I at Multi Cloning Site1 (MCS1) to express YAE1 with a His$_6$ tag along with TEV recognition site and between *Nde*I and *Xho*I into the Multi Cloning Site2 (MCS2) to express ORAOV1 with a *N*-terminal Strep tag along with TEV recognition site. BL21-CodonPlus (DE3)-RIPL competent *E. coli* cells were transformed with the pRSFDuet-1-YAE1-ORAOV1 plasmid and cells were grown in LB or M9 minimal media, containing 1 mM kanamycin and 1 mM chloramphenicol at 37 °C under vigorous shaking up to a cell OD$_{600}$ of 0.6. Protein expression was induced by adding 0.5 mM IPTG and cells were grown overnight at 17 °C. Cells were harvested by centrifugation at 7500×*g* and resuspended in 40 mM sodium phosphate buffer pH 8.0, 300 mM NaCl, 20 mM imidazole, 3 mM DTT, 0.01 mg/mL DNase, 0.01 mg/mL lysozyme, 20 mM MgSO$_4$, protease inhibitor cocktail (Sigma Aldrich) and 10% (v/v) glycerol. Cells disruption was performed on ice by sonication. All the buffers used during the purification were added with protease inhibitor cocktail. The soluble extract, obtained by ultracentrifugation at 40000×*g*, was loaded on a HisTrap FF column (GE Healthcare) and the YAE1-ORAOV1 complex was eluted with 40 mM sodium phosphate buffer pH 8.0, 300 mM NaCl, 400 mM imidazole, and then concentrated with an Amicon Ultra-15 Centrifugal Filter Units with a MWCO of 10 kDa (Millipore), after addition of 5 mM DTT. The sample was buffer exchanged to 20 mM sodium phosphate

buffer pH 7.4, 280 mM NaCl, 6 mM KCl by PD-10 desalting column. The solution was loaded on a StrepTrap HP column (GE Healthcare) and the YAE1-ORAOV1 complex was eluted with 20 mM sodium phosphate buffer pH 7.4, 280 mM NaCl, 6 mM KCl and 2.5 mM desthiobiotin. The heterocomplex was buffer exchanged to 40 mM sodium phosphate buffer pH 8.0, 300 mM NaCl, 5 mM imidazole, 0.2 mM EDTA, 3 mM DTT by PD-10 desalting column. Cleavage of the tags was performed by TEV protease overnight at room temperature. The protein solution was loaded on a HisTrap FF column to separate the digested proteins from the His$_6$-tag and from TEV protease. After concentration the YAE1-ORAOV1 complex was gel filtrated on a HiLoad Superdex 16/600 200 pg column (GE Healthcare) using 50 mM sodium phosphate buffer pH 7.0, 150 mM NaCl, 5 mM DTT as an eluent.

Chemical reconstitution of the YAE1-ORAOV1 complex was performed in an anaerobic chamber ($O_2 < 1$ ppm), by incubating the apo heterocomplex overnight at room temperature in degassed 50 mM Tris buffer pH 8, 150 mM NaCl, 5 mM DTT, with up to an 8-fold excess of FeCl$_3$ and Na$_2$S. Excess of FeCl$_3$ and Na$_2$S was anaerobically removed by passing the mixture on a PD-10 desalting column, and the holo heterocomplex was recovered.

2.5. Production of Cys mutants of ORAOV1 and YAE1-ORAOV1 complex in their apo and holo forms

pENTR-ORAOV1 plasmids containing Cys to Ala mutations for C55, C117 and C65/C70 residues of the ORAOV1 human sequence was acquired from Twist Bioscience. The mutated ORAOV1 gene was then inserted into the pTH34 vector, using the Gateway® technology (Invitrogen) in order to express the mutated ORAOV1 protein. The pRSFDuet-1-YAE1-ORAOV1 plasmid containing Cys to Ala mutations for all the eight cyteines residues of the YAE1 human sequence was acquired from source Twin Helix. Protein production of all mutants were carried out following the same protocols described above for WT ORAOV1 and YAE1-ORAOV1 complex. All mutants were obtained in their apo forms as it occurs for WT ORAOV1 and YAE1-ORAOV1 complex. To obtain the [4Fe-4S] cluster bound form, all the mutants were chemically reconstituted following the same protocol used for WT ORAOV1 and YAE1-ORAOV1 complex.

2.6. Protein, iron, and acid-labile sulfide quantification

Protein quantification was carried out with the Bradford protein assay, using BSA as a standard. Non-heme iron and sulfide contents were determined as described previously [34].

2.7. Biochemical and spectroscopic (UV–visible, far-UV CD, EPR and NMR) analysis

The quaternary structure was analysed by analytical size exclusion chromatography. 0.1 mM samples were loaded on a Superdex 200 10/300 Increase column (GE Healthcare) and 50 mM phosphate buffer pH 7.0, 200 mM NaCl, 5 mM DTT was used as an eluent. The same degassed buffer was used for the analysis of the holo samples. The column was calibrated with a gel filtration marker calibration kit, 6500–66000 Da (Sigma-Aldrich), to estimate the apparent molecular masses of the detected species. Elution profiles were recorded at 280 nm with a flow rate of 0.65 mL/min. SEC-MALS was used to measure the molar masses of apo ORAOV1 and apo YAE1-ORAOV1 complex. The species were separated with a Superdex 200 Increase 10/300 GL column (GE Healthcare) using 50 mM phosphate buffer pH 7.0, 150 mM NaCl, 5 mM DTT as an eluent and then analyzed with a DAWN HELEOS system with a continuous flow rate of 0.6 mL/min.

UV–visible spectra of holo ORAOV1 in degassed 50 mM Tris buffer pH 8.0, 200 mM NaCl, 5 mM DTT, and of holo heterocomplex in 50 mM Tris buffer pH 8.0, 150 mM NaCl, 5 mM DTT were acquired on a Cary 50 Eclipse spectrophotometer. Far-UV CD spectra were collected on a

JASCO J-810C spectropolarimeter with a fused quartz cuvette with 0.1 cm path length (Merck). The far-UV CD spectra were analysed with the DICROPROT software on-line available at https://dicroprot-prabi.ibcp.fr/ to estimate secondary structure composition. The best fitting of the far-UV CD spectra was obtained by using the self-consistent (selcon3) method.

Continuous wave (CW) EPR spectra were recorded before and after the anaerobic reduction of the Fe-S cluster by addition of up to 10 mM sodium dithionite. Protein concentration was in the range 0.3–0.5 mM, in degassed 50 mM Tris buffer pH 8.0, 200 mM NaCl, 5 mM DTT, 10% glycerol (holo ORAOV1), and 50 mM Tris buffer pH 8.0, 150 mM NaCl, 5 mM DTT, 10% glycerol (holo YAE1-ORAOV1 complex). Spectra were acquired at 10 and 45 K, using a Bruker Elexsys 580 spectrometer working at a microwave frequency of ca. 9.36 GHz, equipped with a SHQ cavity and a continuous flow Helium cryostat (ESR900, Oxford instruments) for temperature control. Acquisition parameters were as follows: microwave frequency, 9.36 GHz; microwave power, 2 mW at 10 K and 0.12 mW at 45 K; modulation frequency, 100 kHz; modulation amplitude, 10 G; acquisition time constant, 163.84 ms; number of points 1024; number of scans 4; field range 2000–4000 G.

Standard 1D ^{1}H, 2D ^{1}H-^{15}N HSQC, and steady-state ^{15}N{^{1}H} NOEs NMR experiments were recorded on Bruker AVANCE 500 and 700 MHz spectrometers at 298 K and 310 K. Sample concentration was in the range 0.3–0.5 mM, in 50 mM phosphate buffer pH 7.0, 150 mM NaCl, 5 mM DTT and 10% (v/v) D$_2$O. Spectra were processed using TopSpin (Bruker BioSpin) and analyzed with CARA software.

Paramagnetic 1D ^{1}H NMR experiments [35–38] were recorded on a Bruker Avance 400 MHz spectrometer equipped with a ^{1}H optimized 5 mm probe. Water signal suppression was obtained via fast repetition experiments and water selective irradiation [39]. Experiments were performed using an acquisition time of 50 ms and an overall recycle delay of 85 ms. Sample concentration was in the range 0.4–0.6 mM, in degassed 50 mM Tris buffer pH 8.0, 150 mM NaCl. Squared cosine and exponential multiplications were applied prior to Fourier transformation. Manual baseline correction was performed using polynomial functions.

3. Results and discussion

3.1. Genome browsing and sequence analysis of ORAOV1 and YAE1 proteins

The sequences of 490 proteins (including the template ORAOV1) were identified following a standard procedure reported in the Experimental section. All of them belong to eukaryotic organisms. The aligned sequences have quite a variable length, but a common N-terminal region can be identified with a high residue similarity (~30%, from Phe 18 to Cys 70 in human ORAOV1), indicating that all the selected sequences identify a highly conserved protein family. The conserved region comprises five sequential GX$_3$G motifs forming a **GX$_3$G**-X$_3$-**GX$_3$G**-X$_3$-**GX$_3$G**-X$_3$-**GX$_3$G**-X$_3$-**GX$_3$G** pattern (Fig. 1A), which characterizes this protein family. With the aim of identifying potential Fe-S cluster binding motif (s), we analyzed the conservation of the cysteine residues, which are indeed the most common iron ligands of Fe-S clusters, following previously applied methods [40–42]. ORAOV1 contains four cysteines and three of them are located in the conserved region at the end of the sequential GX$_3$G pattern and organized in a CX$_9$CX$_4$C motif (Fig. 1A). The fourth cysteine is, on the contrary, located 46 residues after the last cysteine of the CX$_9$CX$_4$C motif in a region having lower residue similarity (~20%, comprising residues from Thr 71 to Ser 118 in human ORAOV1, Fig. 1A). The percentage of conservation of the fourth cysteine, i.e. Cys 117, is, however, very high (~90%), the same of that of the first cysteine of the CX$_9$CX$_4$C motif. The other two cysteines of the CX$_9$CX$_4$C motif have slightly lower conservation levels, i.e. ~86% and 78%, respectively. This analysis suggests that the ORAOV1 protein family might bind an iron-sulfur cluster. In order to assess this, we
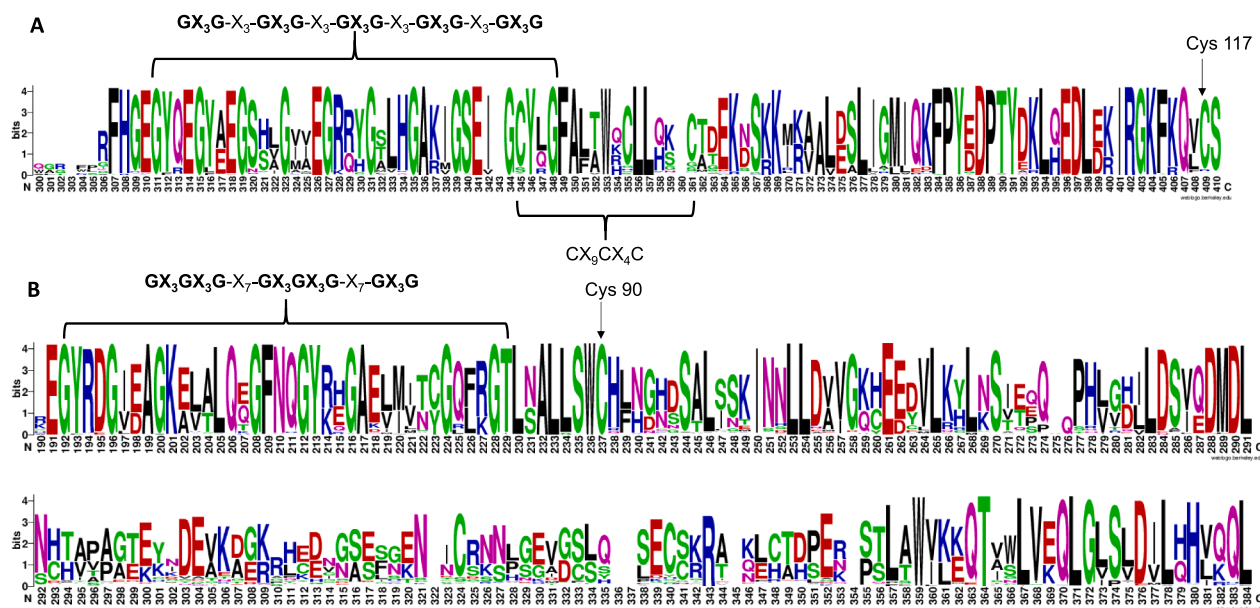
Fig. 1. Sequence analysis of ORAOV1 and YAE1. A multi-sequence alignment of ORAOV1 (A) and YAE1 (B) sequences, selected by BlastP search, was conducted and a weblogo was generated to highlight the conserved sequential GX_3 patterns in ORAOV1 and YAE1, the conserved CX_9CX_4C motif in ORAOV1 and the conserved Cys residues, i.e. Cys 117 in ORAOV1 and Cys 90 in YAE1 (weblogo.berkeley.edu).

produced recombinant human ORAOV1 in *Escherichia coli*. Considering that a hydropathy analysis indicated that human ORAOV1 does not contain *trans*-membrane-spanning helices, the protein was produced in its full-length form.

The same bioinformatics analysis was performed for human YAE1. Even in this case, we identified 490 protein sequences, exclusively in eukaryotes and characterized by a common N-terminal region with a high residue similarity (~30%, from Glu 44 to Lys 119 in human YAE1) that characterizes the YAE1 protein family. The conserved region comprises highly conserved GX_3G motifs, similar to those present in ORAOV1, but differently organized. Two GX_3GX_3G motifs and one GX_3G are sequentially separated by seven residues forming a **GX_3GX_3G-X_7-GX_3GX_3G-X_7-GX_3G** pattern (Fig. 1**B**). Cysteine conservation was also analyzed in YAE1 sequence, which contains eight cysteines. The first cysteine (Cys 90 in human YAE1), located in the conserved region few residues after the GX_3G-based pattern, is fully conserved, while all the others are less conserved and do not identify a characteristic metal-binding motif (Fig. 1**B**). These results suggest that the YAE1 protein family might not bind a Fe-S cluster.

3.2. Structural and Fe-S cluster binding properties of ORAOV1

Recombinant human ORAOV1 was overexpressed in *E. coli*. Both unlabeled and ^{15}N labeled proteins were produced in a culture medium supplemented with iron, in order to promote Fe-S cluster formation *in vivo*. However, after either an aerobic or an anaerobic purification, the protein did not contain any bound cluster, as checked through UV–visible absorption spectroscopy. The final protein sample was highly pure, as checked by SDS-PAGE analysis (Fig. 2A). SEC-MALS analysis showed that aerobically purified apo ORAOV1 eluted as a single peak with a molecular mass of 36 kDa, which corresponds to a roughly dimeric state for the protein, considering that the molecular mass calculated from the aminoacid sequence is 15.354 kDa (Fig. S1). AMS-based alkylation gel shift assay showed that no disulfide bonds are present in aerobically purified apo ORAOV1 (Fig. S1), thus indicating that the dimeric state is not induced by interprotein disulfide bond formation. The far-UV CD spectrum of apo ORAOV1 has the features characteristic of a protein with a large content of α-helical structures (Fig. 2A), i.e. the two typical negative bands at 209 and 224 nm. Analysis of the far-UV CD spectrum

indicated 45% α-helical, 10% β-strand, 12% turn and 33% random coil content. 1D ^1H NMR spectrum of apo ORAOV1 showed a poor chemical shift dispersion of the backbone NH signals, indicative of the presence of unstructured regions. However, up-field shifted signals of methyl groups (Fig. 2**B**) are typical fingerprints of a folded 3D structure. These far-UV CD and NMR-based structural features, which resulted to be the same on both aerobically and anaerobically purified ORAOV1 samples, indicate that apo ORAOV1 contains both α -helical structures and unstructured regions. In order to investigate the structural and dynamical properties of apo ORAOV1 in more details, 2D ^1H-^{15}N HSQC NMR spectra at different temperatures and steady-state $^{15}N\{^1H\}$ NOEs NMR experiments were acquired. In the 2D ^1H-^{15}N HSQC NMR spectra, several signals are clustered in a very narrow ^1H spectral region (7.9–8.6 ppm in the ^1H dimension). Broad lines characterize some of these signals, while others display sharp lines with a high signal-to-noise ratio. Several signals at chemical shift values typical of a well-structured protein conformation are also present and increase in intensity at higher temperatures. However, only 90 of the expected 133 ^{15}N backbone amide resonances (excluding prolines and the first residue) were identified in the 2D ^1H-^{15}N HSQC NMR spectrum of apo ORAOV1 at 310 K (Fig. 2**C**), indicating that several other backbone NHs are overlapped or not detected, as a consequence of the presence of unstructured regions possibly affected by chemical or conformational exchange processes. Moreover, the steady-state $^{15}N\{^1H\}$ NOEs of the detected backbone NH signals showed that several of the signals clustered in the central spectral region are highly flexible (i.e. display motions in the ns-ps time scale), having indeed negative or null $^{15}N\{^1H\}$ NOEs, while the dispersed signals have positive $^{15}N\{^1H\}$ NOEs values, as expected for more rigid conformations (Fig. S2). Overall, the far-UV CD and NMR data indicated that apo ORAOV1 is a protein having both unstructured, flexible region (s) and more rigid, well-structured region(s), characterized by a large α -helical content.

The Fe-S cluster binding properties of ORAOV1 were investigated by chemically reconstituting the purified apo protein. The UV–visible absorption spectra of chemically reconstituted ORAOV1 showed an absorption peak at 410 nm (Fig. 3**A**) that is indicative of a $[4Fe-4S]^{2+}$ cluster. UV–visible CD spectrum of chemically reconstituted ORAOV1 is also indicative of the presence of a $[4Fe-4S]^{2+}$ bound cluster (Fig. S2). It shows indeed very weak bands, as usually observed in [4Fe-4S] proteins,
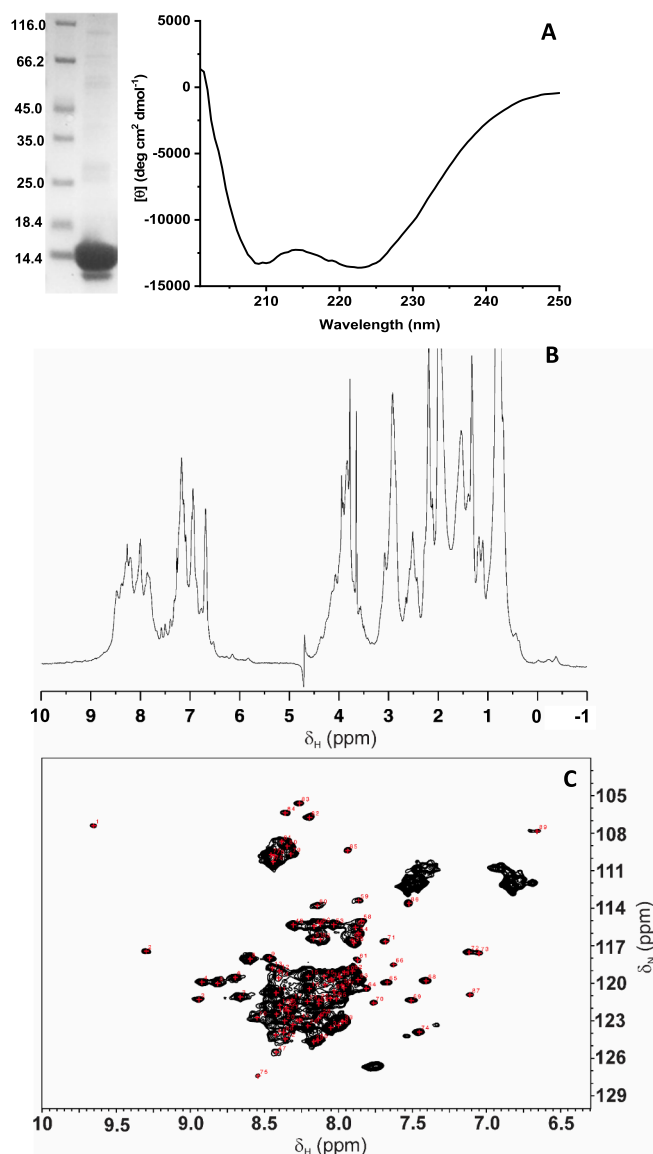
Fig. 2. Far-UV CD and NMR spectra of purified apo ORAOV1. (A) Far-UV CD spectrum in mean residue ellipticity ([θ]) and SDS-PAGE of aerobically purified apo ORAOV1 are reported. 1D ^{1}H NMR (B) and 2D ^{1}H-^{15}N HSQC NMR (C) spectra of aerobically purified apo ORAOV1 acquired at 310 K.

Fig. 3. ORAOV1 binds a [4Fe-4S] cluster. (A) UV–visible absorption spectrum of chemically reconstituted ORAOV1. ε value is based on dimeric protein concentration. (B) Analytical gel filtration profiles of apo purified (black) and chemically reconstituted (red) ORAOV1. (C) EPR spectrum of dithionite-reduced, chemically reconstituted ORAOV1 recorded at 10 K. g values are indicated.

which typically display CD spectra of low or even no intensity compared to the well-structured CD spectra for proteins containing [2Fe–2S] clusters [43,44]. From analytical gel filtration, we observed that cluster binding does not affect the quaternary protein structure, as both chemically reconstituted and purified apo forms eluted as a single peak with the same retention volume (Fig. 3B). Iron and acid-labile sulfide analyses indicated an Fe:S^{2-} ratio close to 1:1 (Table 1). Moreover, the analytical data on three independent preparations indicated a 4.3 ± 0.1 Fe and 3.8 ± 0.1 S^{2-} content per dimer, consistent with the presence of ~1.0 [4Fe-4S] cluster per dimer (Table 1). This data is in agreement with the UV–visible absorption value of $\varepsilon_{400} = 12.4$ mM^{-1} cm^{-1} (obtained considering the dimeric ORAOV1 concentration), which indicates indeed that ~80% of dimeric ORAOV1 binds a [4Fe-4S]$^{2+}$ cluster, on the basis of the typical ε_{400} value of 15 ± 2 mM^{-1} cm^{-1} for one [4Fe-4S]$^{2+}$ cluster [45].

While chemically reconstituted ORAOV1 showed no EPR signals, samples frozen within 5 s from dithionite addition showed a rhombic set of resonances with $g_1 = 2.04$, $g_2 = 1.93$ and $g_3 = 1.86$ (Fig. 3C). The signal was assigned to an electron spin state S = 1/2 of a [4Fe-4S]$^+$
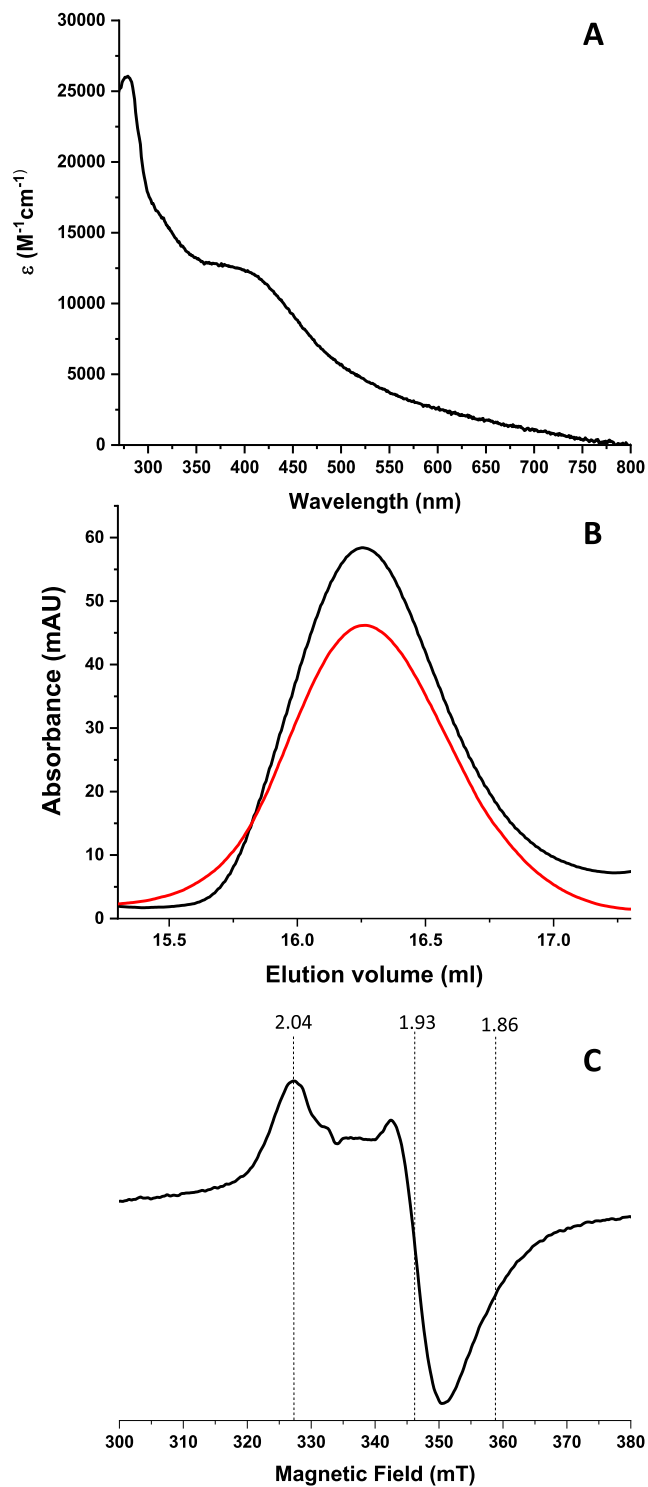
cluster rather than of a [2Fe-2S]$^+$ cluster, based on electron spin relaxation properties. Indeed, the resonances are detectable without significant broadening at 10 K, while broaden beyond detection at 45 K. This indicates fast relaxation, which is typical of S = 1/2 [4Fe-4S]$^+$ clusters, whereas S = 1/2 [2Fe-2S]$^+$ clusters are much slower relaxing

Table 1

Acid-labile sulfide analyses of ORAOV1 and YAE1-ORAOV1 complex. Fe and S measurements are the averages of three independent samples.

Sample	Fe[a]	S^{2-a}
Chemically reconstituted ORAOV1	4.3 ± 0.1	3.8 ± 0.1
Chemically reconstituted YAE1-ORAOV1 complex	3.6 ± 0.1	3.5 ± 0.1

[a] Fe and acid-labile S^{2-} measurements are reported as mol Fe or S^{2-} per mol of dimeric ORAOV1 or heterodimeric YAE1-ORAOV1.

and their EPR signals remain still sharp at 45 K and can be easily power saturated at 10 K. Thus, EPR data of reduced, chemically reconstituted ORAOV1 show a paramagnetic species due to the presence of a S = 1/2 $[4Fe-4S]^+$ bound cluster.

In conclusion, the analytical and spectroscopic data indicated that ORAOV1 is a homodimer with α -helical and flexible unstructured regions able to bind a $[4Fe-4S]^{2+}$ cluster and that protein dimerization is independent by [4Fe-4S] cluster binding.

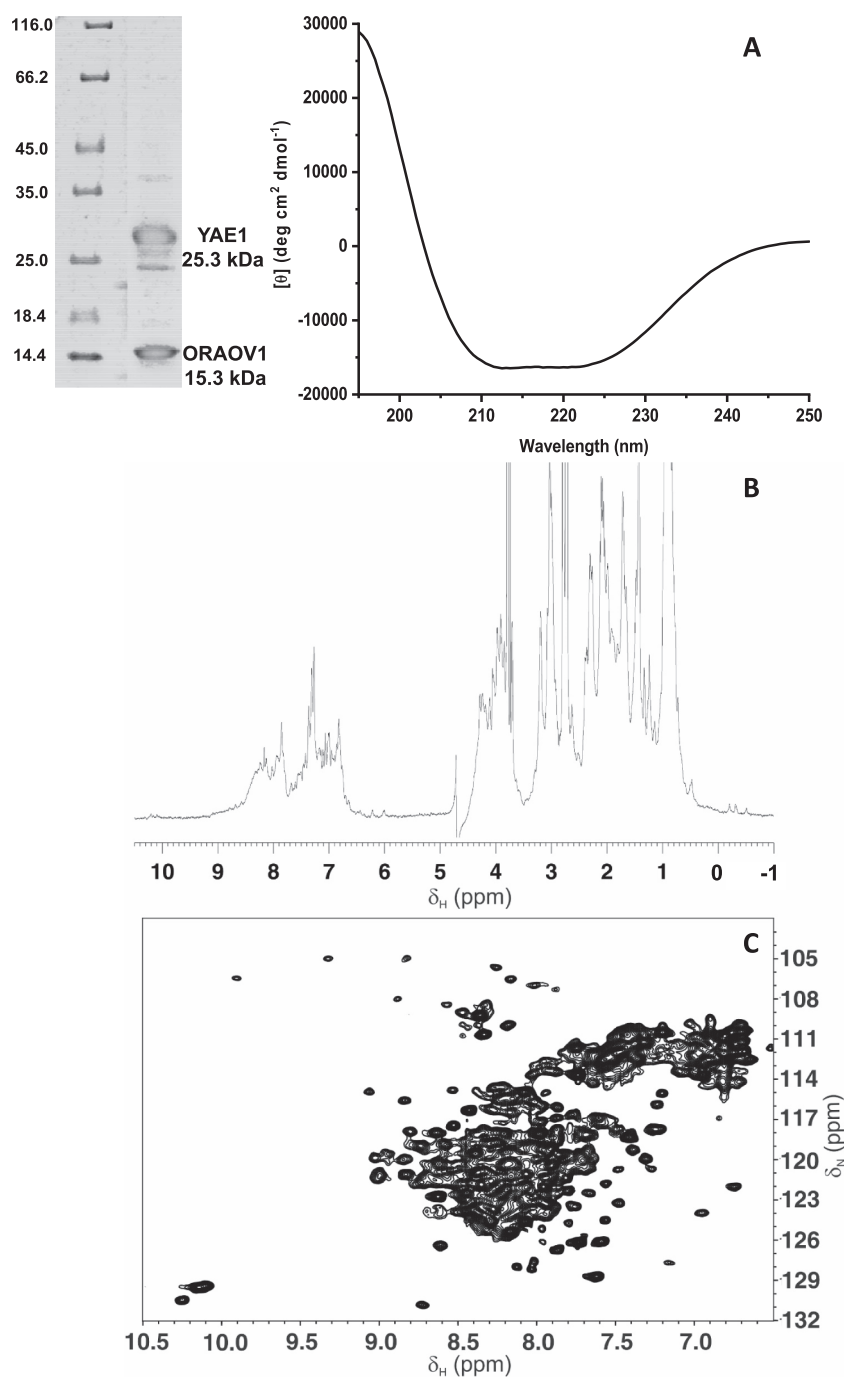**Fig. 4.** Far-UV CD and NMR spectra of purified apo YAE1-ORAOV1 complex. (A) Far-UV CD spectrum in mean residue ellipticity ([θ]) and SDS-PAGE of aerobically purified apo YAE1-ORAOV1 complex are reported. 1D ¹H NMR (B) and 2D ¹H-¹⁵N HSQC NMR (C) spectra of aerobically purified apo YAE1-ORAOV1 complex acquired at 310 K.

3.3. Structural and Fe-S cluster binding properties of the YAE1-ORAOV1 complex

The YAE1-ORAOV1 complex was obtained by co-expressing the two proteins in the *E. coli* host (see Experimental section for details). This approach was followed since it has not been possible to form the heterocomplex *in vitro* from the isolated proteins, as YAE1 alone is insoluble in all the tested experimental conditions. Upon co-expression of the two proteins, Strep-tag ORAOV1 co-elutes with His$_6$-tag YAE1 in the first step of His$_6$-tag affinity purification (Fig. S1) as a colorless complex, thus with no cluster bound. The UV–visible absorption spectrum did not show indeed any band in the visible region, as expected when Fe-S clusters are bound. The apo heterocomplex, after the removal of Strep- and His$_6$-tags, was isolated at a high purity level, as checked by SDS-PAGE analysis (Fig. 4A). SEC-MALS analysis showed that the purified apo heterocomplex eluted as a single peak with a molecular mass of 42 kDa, which corresponds to the formation of a heterodimeric complex, considering that the molecular mass calculated from the aminoacid sequence is 15.354 kDa for ORAOV1 and 25.299 kDa for YAE1 (Fig. S1). The far-UV CD spectrum of the purified apo heterocomplex show the typical negative bands characteristic of α-helical structures, resulting very similar to that of ORAOV1 (Fig. 4A). Analysis of the far-UV CD spectrum indicated a 47% α-helical, 12% β -strand, 10% turn and 31% random coil content. These far-UV CD-based structural features are the same on both aerobically and anaerobically purified apo heterocomplex samples. The 1D ^{1}H and 2D ^{1}H-^{15}N HSQC NMR spectra of the purified apo heterocomplex share some similarity with those of ORAOV1. Indeed, also the heterocomplex shows some backbone NH signals with a poor dispersion, indicative of unstructured region(s), as well as NH signals with dispersed chemical shift values and up-field shifted signals of methyl groups, both the latter features typical of a well-structured protein conformation (Fig. 4B and 4C). Far-UV CD and NMR data thus indicated that the apo heterocomplex has a conformation composed by both unstructured region(s) and well-structured α -helical region(s), similarly to what observed in apo ORAOV1. Superimposing the 2D ^{1}H-^{15}N HSQC NMR maps of the purified apo heterocomplex with that of purified apo ORAOV1, it resulted that the backbone NH signals of ORAOV1 do not overlap with the signals of the heterocomplex, indicating that ORAOV1 in the heterocomplex changes its structural environment (Fig. S3). This is expected considering the major change of the quaternary structure of ORAOV1, which goes from a homodimeric state to a heterodimeric state.

The purified apo heterocomplex was chemically reconstituted (see Experimental section for details) and was spectroscopically characterized by UV–visible, EPR and paramagnetic 1D ^{1}H NMR spectroscopies. As observed for ORAOV1, analytical gel filtration showed that cluster binding does not affect the quaternary structure of the heterocomplex, as both chemically reconstituted and apo forms eluted as a single peak with the same retention volume. The UV–visible absorption spectrum of the chemically reconstituted heterocomplex showed an absorption peak at 410 nm (Fig. 5A) that is indicative of a [4Fe-4S]$^{2+}$ cluster. The UV–visible absorption value of $\varepsilon_{400} = 15.0$ mM^{-1} cm^{-1} (obtained considering the heterocomplex concentration) indicates that a [4Fe-4S]$^{2+}$ cluster is bound to the heterocomplex. This agrees with the iron and acid-labile sulfide analysis that indicates the presence of ~0.9 [4Fe-4S] cluster per heterocomplex (Table 1).

As observed for ORAOV1 alone, EPR spectra acquired on the chemically reconstituted heterocomplex showed no signals, but, upon its dithionite reduction, a rhombic set of resonances with $g_1 = 2.04$, $g_2 = 1.93$ and $g_3 = 1.86$ appeared (Fig. 5B). These resonances are the same as those observed upon reduction of the chemically reconstituted ORAOV1. They also have the same relaxation properties being observable without significant broadening at 10 K and broadening beyond detection at 45 K. Thus, the EPR data are in agreement with the presence of a S = 1/2 [4Fe-4S]$^+$ cluster.

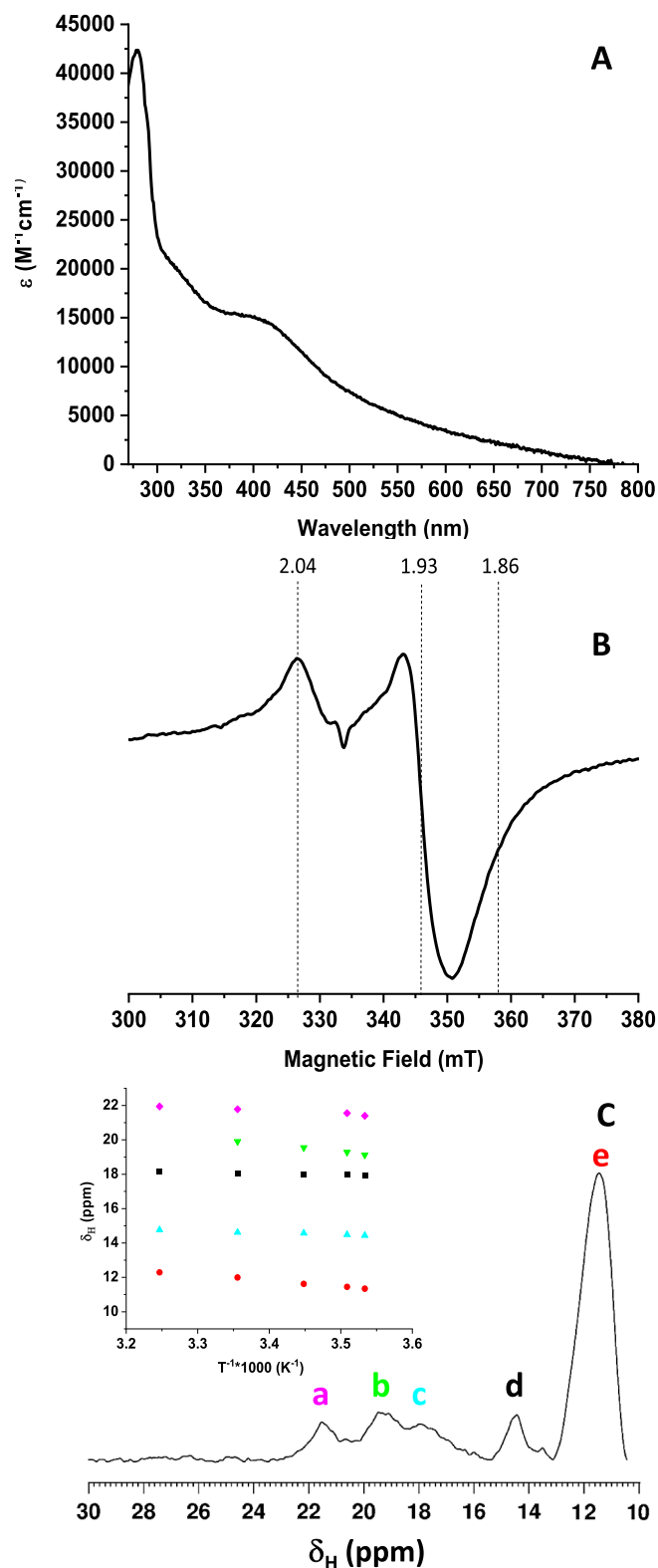The paramagnetic 1D ^{1}H NMR spectrum of the chemically

Fig. 5. The YAE1-ORAOV1 complex binds a [4Fe-4S] cluster. (A) UV–visible absorption spectrum of chemically reconstituted YAE1-ORAOV1 complex. ε value is based on heterodimeric complex concentration. (B) EPR spectrum of dithionite-reduced, chemically reconstituted YAE1-ORAOV1 complex recorded at 10 K. g values are indicated. (C) Paramagnetic 1D ^{1}H NMR of chemically reconstituted YAE1-ORAOV1 complex recorded at 285 K. In the inset, temperature dependences of the hyperfine-shifted signals (a, b, c, d and e) of chemically reconstituted YAE1-ORAOV1 complex are reported.

reconstituted heterocomplex showed hyperfine-shifted signals at 11.5, 14.5, 18.0, 19.2 and 21.5 ppm (Fig. 5C). All these signals show an anti-Curie temperature dependence (Fig. 5C inset). The chemical shift values of the hyperfine-shifted signals, their anti-Curie temperature dependence, and their linewidths are typical of βCH_2 signals of Cys residues bound to a $[4Fe-4S]^{2+}$ cluster with an $S = 0$ electronic ground state, with the paramagnetism arising from excited states of the electron spin ladder, partially populated at room temperature [37].

3.4. Site-directed mutagenesis studies on YAE1-ORAOV1 complex

Bioinformatic sequence analysis on ORAOV1 and YAE1 suggested that, while YAE1 does not have a metal-binding consensus motif, ORAOV1 has a metal-binding motif formed by four cysteines organized in a $CX_9CX_4CX_{46}C$ motif. Consistent with this, we found that ORAOV1 binds a $[4Fe-4S]^{2+}$ cluster. In order to investigate how the latter cluster is bound in the YAE1-ORAOV1 complex, we have performed site-directed mutagenesis studies. First, in order to support that the $CX_9CX_4CX_{46}C$ motif is responsible of $[4Fe-4S]^{2+}$ cluster binding in ORAOV1, single and double cysteine mutants of the ORAOV1 cluster binding motif (C55A, C117A and C65A/C70A) were produced and their Fe-S cluster binding properties investigated by UV–visible and EPR spectroscopies. The UV–visible spectrum of the C55A mutant (Fig. 6A) shows a significant decrease in intensity of the band at 400 nm, indicating a lower fraction (25% less) of [4Fe-4S] cluster bound to ORAOV1. Thus, although cluster binding to ORAOV1 is not abolished by the C55A mutation, this mutation affects the cluster/protein ratio. This is also consistent with the iron and acid-labile sulfide analysis that indicated the presence of ~ 0.7 [4Fe-4S] cluster per dimer in the C55A mutant. These results suggest that Cys 55 is relevant to promote cluster binding, since its removal reduces the cluster binding ability, although it does not abolish it, similarly to what already reported for several other systems where cysteines are mutated to alanines [46–50]. The UV–visible spectra of the other two mutants, i.e. C117A and C65/70A, also differ from that of WT ORAOV1 since both showed the band at 400 nm broader than that of WT ORAOV1 and also a broad band at ~ 650 nm not observed in the spectrum of WT ORAOV1 (Fig. 6A). The latter band is typically observed when, in the chemical reconstitution, Fe^{3+}-containing aggregates are formed as a consequence of an inefficient chemical reconstitution (note that we applied the same chemical reconstitution procedure on the mutants and on WT ORAOV1), and they are not fully removed by the PD-10 desalting column [43]. Therefore, the UV–visible spectral features of the C117A and C65/70A mutants are essentially derived from adventitious association of Fe and sulfide on the protein that are not removed by the desalting column, at variance with what observed for WT ORAOV1 and the C55A mutant. The latter two proteins indeed do not show these spectral features (a very faint band at ~ 650 nm is, however, observed in the C55A mutant), but showed UV–vis spectra typical of a [4Fe-4S] cluster-bound protein. Overall, the UV–vis data thus support that C117, C65 and C70 are relevant to promote cluster binding, as found for C55. EPR spectra (Fig. 6B) confirms a role of the four cysteines in cluster binding as the mutants show multiple EPR signals with very low intensity at variance with the EPR spectrum of WT ORAOV1, which shows, on the contrary, the presence of only one intense EPR signal. Thus, the EPR data indicate a profound difference of WT vs. mutants in cluster coordination properties, supporting that C55, C117, C65 and C70 are relevant to promote cluster binding. The first three cysteines of the conserved $CX_9CX_4CX_{46}C$ motif immediately follow the sequential GX_3 motifs of ORAOV1 (being C55 even included at the C-side of latter motif), which are responsible for the interaction between ORAOV1 and YAE1 as well as for Rli1 (the ABCE1 yeast homolog) maturation [30]. Thus, cluster binding on ORAOV1 is located close to the conserved region responsible for the heterocomplex function in the CIA machinery, supporting that a [4Fe-4S] cluster bound molecule of ORAVO1, once complexed with YAE1, might promote the cluster incorporation in Rli1.
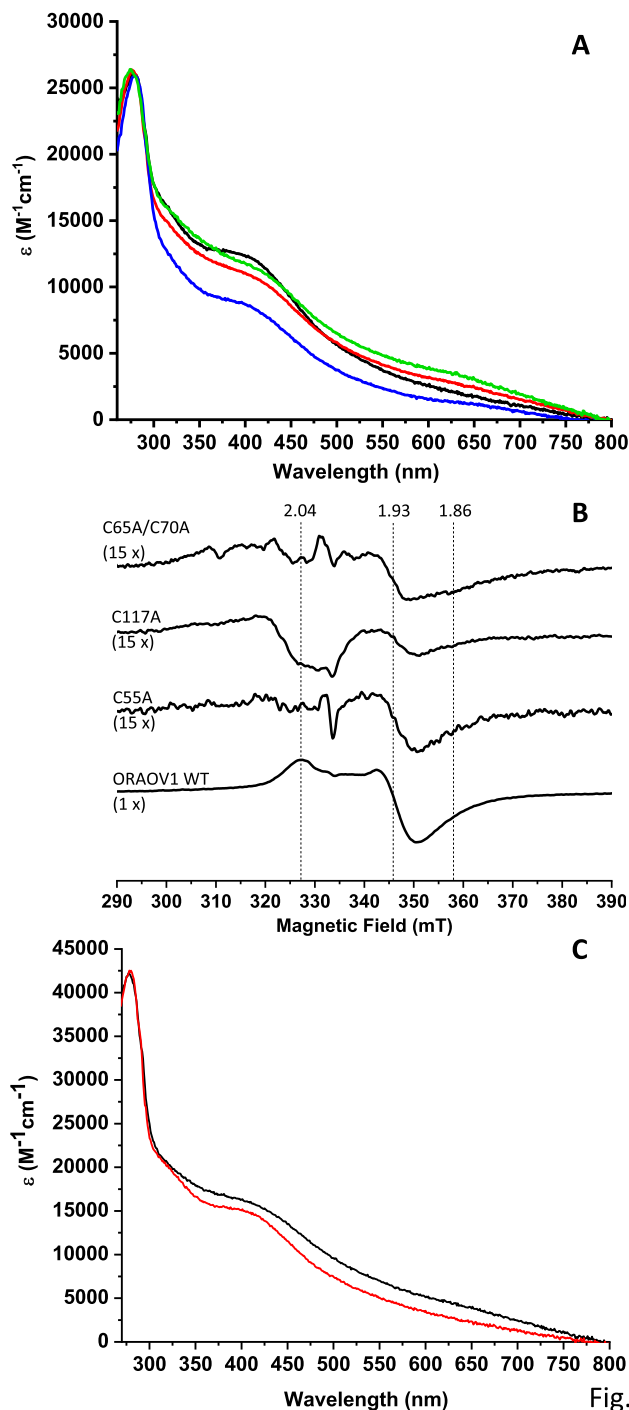
Fig. 6

Fig. 6. Site-directed mutagenesis studies indicate that ORAOV1 binds a [4Fe-4S] cluster in the YAE1-ORAOV1 complex. (A) UV–visible absorption spectra of chemically reconstituted C55A (blue), C117A (green), C65A/C70A (red) ORAOV1 mutants. ε value is based on dimeric complex concentration. The UV–visible spectrum of WT ORAOV1 (black) is reported for comparison. (B) EPR spectra of dithionite-reduced, chemically reconstituted ORAOV1 mutants recorded at 10 K. The EPR spectrum of WT ORAOV1 (black) is reported for comparison. The g values of WT ORAOV1 are indicated. (C) UV–visible absorption spectrum of chemically reconstituted Cys-mutated YAE1-ORAOV1 complex (black line) and WT YAE1-ORAOV1 (red line). ε value is based on heterodimeric complex concentration.

What this mutational data cannot conclusively address is whether all or just some of the four cysteines are the cluster ligands since the data do not allow us to distinguish whether the cluster is bound exclusively to one of the two subunits of homodimer ORAOV1 or is bridged between the subunits of the homodimer. Thus, it is possible that the spectroscopic features observed on some mutants reflect the fact that some of the cysteines coordinate the [4Fe-4S] cluster, while others are involved in the [4Fe-4S] cluster acquisition without being directly involved in its coordination. Iron and acid-labile sulfide analysis on WT ORAVO1, which indicated the presence of ~1.0 [4Fe-4S] clusters per dimer, also does not provide a definitive answer on this aspect. Indeed, the presence of one cluster per dimer in ORAOV1 might be interpreted either as a cluster bridging the two subunits or as an inefficiency of the *in vitro* Fe-S cluster reconstitution process, considering that ORAOV1 homodimer is not a physiological species. Thus, in the latter case it is possible that, once a subunit of the ORAOV1 homodimer binds one cluster, the binding of the [4Fe-4S] cluster to the other subunit is disfavored. However, the not-bridged cluster mode of binding is supported by the fact that the dimeric state of ORAOV1 is independent of cluster binding (Fig. 3**B**), at variance with what usually occurs in dimers with a bridged Fe-S cluster, which, indeed, are formed only upon cluster binding through two cysteine ligands from each subunit [51–53].

As following step, we mutated all the eight cysteines of YAE1 into Ala in the plasmid used previously to co-express YAE1 and ORAOV1 proteins. The Cys-mutated YAE1-ORAOV1 complex was then purified from *E. coli* cells in the apo form and its Fe-S cluster binding properties were investigated by chemically reconstituting it and performing UV–visible and paramagnetic NMR experiments. The Cys to Ala mutations do not affect the structural properties of the heterocomplex, which in both its apo and chemically reconstituted forms, is a heterodimer with a predominant content of α-helical secondary structure (Fig. S4). The UV–visible absorption spectrum of the chemically reconstituted Cys-mutated YAE1-ORAOV1 complex is similar to that of the WT complex (Fig. 6**C**), indicating that the binding of the [4Fe-4S] cluster occurs also in the absence of all the cysteines of YAE1. This result indicates that YAE1 is not essential for [4Fe-4S] cluster binding in the YAE1-ORAOV1 complex. The paramagnetic 1D ^{1}H NMR spectrum of the chemically reconstituted Cys-mutated YAE1-ORAOV1 complex (Fig. S4) is also in agreement with this model, showing indeed the presence of hyperfine-shifted signals typical of a [4Fe-4S]$^{2+}$ cluster-bound species. However, it shows some differences with respect to the spectrum of the WT heterocomplex, indicating that the cluster binding properties of the heterocomplex are slightly modified by the cysteines mutation on YAE1. The [4Fe-4S] cluster binding stability is also modified in the Cys-mutated YAE1-ORAOV1 complex with respect to the WT heterocomplex, as evidenced by the poor signal-to-noise ratio in the paramagnetic 1D ^{1}H NMR spectrum (Fig. S4), because of the loss of the cluster during the acquisition of the NMR experiments. Overall, the latter results indicated that the YAE1 cysteines mutation affects the cluster binding on the heterocomplex without abolishing it, potentially implicating some residue(s) of YAE1 in cluster ligation, mimicking previously observed, bridged [4Fe-4S] or [2Fe-2S] cluster-bound dimers [18,51–55].

In conclusion, we found that: i) ORAOV1 is able to bind a [4Fe-4S] cluster, likely being the cluster not bridged between the two subunits of the homodimer, which thus results not efficiently bound (50% [4Fe-4S] cluster loading) consistent with not being ORAOV1 alone a physiological species; ii) the physiological heterodimeric species is, on the contrary, efficiently chemically reconstituted with one [4Fe-4S] cluster; iii) the [4Fe-4S] cluster binding is not abolished in the Cys-mutated YAE1 complexed to ORAOV1; iv) the EPR spectrum of chemically reconstituted heterocomplex is the same as that observed in the chemically reconstituted ORAOV1. All these findings favor a model in which ORAOV1 is the only culprit for the [4Fe-4S] cluster binding to the heterocomplex. However, only a structural model of the heterocomplex can provide the definitive answer to this behavior. Indeed, it will be able to discriminate between an active role of YAE1 in cluster coordination and

an indirect role of YAE1 in modulating the properties of a [4Fe-4S] cluster coordinated exclusively by ORAVO1.

4. Conclusions

The maturation of the human ABC protein, ABCE1, depends on the 'CIA adapter complex' composed of ORAOV1 and YAE1 [30]. The proposed model is that YAE1 and ORAOV1 form a heterocomplex able to carry apo ABCE1 to the CIA targeting complex in order to promote the insertion of [4Fe-4S] clusters into ABCE1. Specifically, ORAOV1 interacts with the CIA targeting complex and not with ABCE1, while YAE1 interacts with ABCE1 [28,30]. Thus, YAE1-ORAOV1 complex acts as a bridge between the CIA targeting complex and ABCE1. No information was available establishing whether the YAE1-ORAOV1 complex has a role in the Fe-S cluster binding and insertion into ABCE1. Our study showed that ORAOV1 both as isolated protein and complexed with YAE1 binds a [4Fe-4S]$^{2+}$ cluster. Overall, the data support a model that the [4Fe-4S] cluster in ORAOV1 is bound by a conserved cluster binding motif, while YAE1, which has not a metal-binding consensus motif, is not required for the [4Fe-4S]$^{2+}$ cluster binding in the YAE1-ORAOV1 hetero-complex. On this basis, we can suggest that the heterocomplex might actively participate in the [4Fe-4S] cluster insertion into ABCE1 thanks to the [4Fe-4S] cluster binding properties of ORAOV1.

The approach, used here on ORAOV1 and YAE1 proteins, which combines bioinformatics, site-directed mutagenesis, NMR, EPR and UV–visible spectroscopies, was thus able to provide information on the possible ability of the 'CIA adapter complex' to play an active role in inserting [4Fe-4S] clusters into ABCE1. More detailed, structural data will be then required to provide a conclusive picture at the atomic level on how the interaction between the two proteins could create the structure to bind and transfer the [4Fe-4S] cluster to ABCE1.

CRediT authorship contribution statement

Nihar Ranjan Prusty: Investigation, Formal analysis. **Francesca Camponeschi:** Investigation, Validation. **Simone Ciofi-Baffoni:** Conceptualization, Supervision, Writing - original draft, Visualization. **Lucia Banci:** Conceptualization, Supervision, Resources, Funding acquisition.

Declaration of Competing Interest

The authors declare that they have no known competing financial interests or personal relationships that could have appeared to influence the work reported in this paper.

Appendix A. Supplementary data

Supplementary data to this article can be found online at https://doi.org/10.1016/j.ica.2021.120252.

References

[1] H. Beinert, R.H. Holm, E. Munck, Science 277 (1997) 653–659.
[2] D.C. Rees, J.B. Howard, Science 300 (2003) 929–931.
[3] R. Lill, Nature 460 (2009) 831–838.
[4] R. Lill, Biol. Chem. 401 (2020) 855–876.

[5] N. Maio, T.A. Rouault, Trends Biochem. Sci. 45 (2020) 411–426.

[6] S. Ciofi-Baffoni, V. Nasta, L. Banci, Metallomics 10 (2018) 49–72.

[7] V.D. Paul, R. Lill, BBA 1853 (2015) 1528–1539.

[8] T.A. Rouault, Biometals 32 (2019) 343–353.

[9] K.S. Kim, N. Maio, A. Singh, T.A. Rouault, Hum. Mol. Genet. 27 (2018) 837–852.

[10] O. Stehling, D.J. Netz, B. Niggemeyer, R. Rosser, R.S. Eisenstein, H. Puccio, A. J. Pierik, R. Lill, Mol. Cell. Biol. 28 (2008) 5517–5528.

[11] O. Stehling, J.H. Jeoung, S.A. Freibert, V.D. Paul, S. Bänfer, B. Niggemeyer, R. Rösser, H. Dobbek, R. Lill, Proc. Natl. Acad. Sci. USA 115 (2018) E9085–E9094.

[12] F. Camponeschi, N.R. Prusty, S.A.E. Heider, S. Ciofi-Baffoni, L. Banci, J. Am. Chem. Soc. 142 (2020) 10794–10805.

[13] L. Banci, F. Camponeschi, S. Ciofi-Baffoni, R. Muzzioli, J. Am. Chem. Soc. 137 (2015) 16133–16134.

[14] D.J. Netz, M. Stumpfig, C. Dore, U. Muhlenhoff, A.J. Pierik, R. Lill, Nat. Chem. Biol. 6 (2010) 758–765.

[15] L. Banci, I. Bertini, V. Calderone, S. Ciofi-Baffoni, A. Giachetti, D. Jaiswal, M. Mikolajczyk, M. Piccioli, J. Winkelmann, PNAS 110 (2013) 7136–7141.

[16] L. Banci, S. Ciofi-Baffoni, M. Mikolajczyk, J. Winkelmann, E. Bill, M.E. Pandelia, J. Biol. Inorg. Chem. 18 (2013) 883–893.

[17] L. Banci, S. Ciofi-Baffoni, K. Gajda, R. Muzzioli, R. Peruzzini, J. Winkelmann, Nat. Chem. Biol. 11 (2015) 772–778.

[18] D.J. Netz, A.J. Pierik, M. Stumpfig, E. Bill, A.K. Sharma, L.J. Pallesen, W.E. Walden, R. Lill, J. Biol. Chem. 287 (2012) 12365–12378.

[19] K. Gari, A.M. Leon Ortiz, V. Borel, H. Flynn, J.M. Skehel, S.J. Boulton, Science 337 (2012) 243–245.

[20] O. Stehling, A.A. Vashisht, J. Mascarenhas, Z.O. Jonsson, T. Sharma, D.J. Netz, A. J. Pierik, J.A. Wohlschlegel, R. Lill, Science 337 (2012) 195–199.

[21] V. Maione, D. Grifagni, F. Torricella, F. Cantini, L. Banci, J. Biol. Inorg. Chem. 25 (2020) 501–508.

[22] M. Seki, Y. Takeda, K. Iwai, K. Tanaka, J. Biol. Chem. 288 (2013) 16680–16689.

[23] S.A. Kassube, N.H. Thomä, Nat. Struct. Mol. Biol. 27 (2020) 735–742.

[24] T. Becker, S. Franckenberg, S. Wickles, C.J. Shoemaker, A.M. Anger, J.P. Armache, H. Sieber, C. Ungewickell, O. Berninghausen, I. Daberkow, A. Karcher, M. Thomm, K.P. Hopfner, R. Green, R. Beckmann, Nature 482 (2012) 501–506.

[25] G. Kispal, K. Sipos, H. Lange, Z. Fekete, T. Bedekovics, T. Janáky, J. Bassler, D. J. Aguilar Netz, J. Balk, C. Rotte, R. Lill, EMBO J. 24 (2005) 589–598.

[26] A. Yarunin, V.G. Panse, E. Petfalski, C. Dez, D. Tollervey, E.C. Hurt, EMBO J. 24 (2005) 580–588.

[27] A. Karcher, K. Büttner, B. Märtens, R.P. Jansen, K.P. Hopfner, Structure 13 (2005) 649–659.

[28] C. Zhai, Y. Li, C. Mascarenhas, Q. Lin, K. Li, I. Vyrides, C.M. Grant, B. Panaretou, Oncogene 33 (2014) 484–494.

[29] D. Barthelme, U. Scheele, S. Dinkelaker, A. Janoschka, F. Macmillan, S.V. Albers, A.J. Driessen, M.S. Stagni, E. Bill, W. Meyer-Klaucke, V. Schünemann, R. Tampé, J. Biol. Chem. 282 (2007) 14598–14607.

[30] V.D. Paul, U. Muhlenhoff, M. Stumpfig, J. Seebacher, K.G. Kugler, C. Renicke, C. Taxis, A.C. Gavin, A.J. Pierik, R. Lill, Elife 4 (2015), e08231.

[31] J.D. Thompson, D.G. Higgins, T.J. Gibson, Nucleic Acids Res. 22 (1994) 4673–4680.

[32] G.E. Crooks, G. Hon, J.M. Chandonia, S.E. Brenner, Genome Res. 14 (2004) 1188–1190.

[33] L. Banci, I. Bertini, C. Cefaro, S. Ciofi-Baffoni, A. Gallo, M. Martinelli, D.P. Sideris, N. Katrakili, K. Tokatlidis, Nat. Struct. Mol. Biol. 16 (2009) 198–206.

[34] L. Banci, I. Bertini, S. Ciofi-Baffoni, F. Boscaro, A. Chatzi, M. Mikolajczyk, K. Tokatlidis, J. Winkelmann, Chem. Biol. 18 (2011) 794–804.

[35] S. Ciofi-Baffoni, A. Gallo, R. Muzzioli, M. Piccioli, J. Biomol. NMR 58 (2014) 123–128.

[36] F. Camponeschi, R. Muzzioli, S. Ciofi-Baffoni, M. Piccioli, L. Banci, J. Mol. Biol. 431 (2019) 4514–4522.

[37] L. Banci, F. Camponeschi, S. Ciofi-Baffoni, M. Piccioli, J. Biol. Inorg. Chem. 23 (2018), 687 687.

[38] F. Arnesano, L. Banci, I. Bertini, S. Ciofi-Baffoni, T. de Lumley Woodyear, C. M. Johnson, P.D. Barker, Biochemistry 39 (2000) 1499–1514.

[39] S.L. Patt, B.D. Sykes, J. Chem. Phys. 56 (1972) 3182.

[40] Y. Valasatava, A. Rosato, L. Banci, C. Andreini, Bioinformatics 32 (2016) 2850–2852.

[41] C. Andreini, V. Putignano, A. Rosato, L. Banci, Metallomics 10 (2018) 1223–1231.

[42] V. Putignano, A. Rosato, L. Banci, C. Andreini, Nucleic Acids Res. 46 (2018) D459–D464.

[43] S.A. Freibert, B.D. Weiler, E. Bill, A.J. Pierik, U. Muhlenhoff, R. Lill, Methods Enzymol. 599 (2018) 197–226.

[44] D.T. Mapolelo, B. Zhang, S.G. Naik, B.H. Huynh, M.K. Johnson, Biochemistry 51 (2012) 8071–8084.

[45] M. Roland, J. Przybyla-Toscano, F. Vignols, N. Berger, T. Azam, L. Christ, V. Santoni, H.C. Wu, T. Dhalleine, M.K. Johnson, C. Dubos, J. Couturier, N. Rouhier, J. Biol. Chem. 295 (2020) 1727–1742.

[46] J. Tamarit, C. Gerez, C. Meier, E. Mulliez, A. Trautwein, M. Fontecave, J. Biol. Chem. 275 (2000) 15669–15675.

[47] D.J. Netz, H.M. Genau, B.D. Weiler, E. Bill, A.J. Pierik, R. Lill, Biochem. J. 473 (2016) 2073–2085.

[48] Y. Zhang, C. Yang, A. Dancis, E. Nakamaru-Ogiso, J. Biochem. 161 (2017) 67–78.

[49] E. Urzica, A.J. Pierik, U. Muhlenhoff, R. Lill, Biochemistry 48 (2009) 4946–4958.

[50] K.S. Hewitson, S. Ollagnier-de Choudens, Y. Sanakis, N.M. Shaw, J.E. Baldwin, E. Münck, P.L. Roach, M. Fontecave, J. Biol. Inorg. Chem. 7 (2002) 83–93.

[51] V. Nasta, D. Suraci, S. Gourdoupis, S. Ciofi-Baffoni, L. Banci, FEBS J. 287 (2020) 2312–2327.

[52] V. Nasta, S. Da Vela, S. Gourdoupis, S. Ciofi-Baffoni, D.I. Svergun, L. Banci, Sci. Rep. 9 (2019) 18986.

[53] V. Nasta, A. Giachetti, S. Ciofi-Baffoni, L. Banci, BBA 1861 (2017) 2119–2131.

[54] A. Jain, A. Singh, N. Maio, T.A. Rouault, Hum. Mol. Genet. (2020).

[55] S. Gourdoupis, V. Nasta, V. Calderone, S. Ciofi-Baffoni, L. Banci, J. Am. Chem. Soc. 140 (2018) 14401–14412.